Extended Data Figures & Legends

Extended Data Fig. 1 | Purification of Cx43 GJIChs and workflow of cryo-EM image processing of Cx43-WT GJICh in detergents and nanodiscs.

a, Gel filtration profiles of Cx43-WT (green) and Cx43-M257 (orange) in detergents. Asterisks in red and black indicate peaks presumed to be GJIChs and hemichannels, respectively.

b, SDS-PAGE gel of purified Cx43-WT (left) and Cx43-M257 (middle) in detergents, and Cx43-WT in nanodiscs (right). MSP1E3D1 is indicated by an arrow.

c, Mass spectrometry analysis of purified Cx43-WT. The first methionine residue was not detected in any identified N-terminal peptides. The N-terminal G2 was acetylated (Ac-G) in two peptides and highlighted in red color.

d,e, Workflows of cryo-EM image processing of Cx43-WT GJICh at pH 8.0 in detergents (**d**) and in nanodiscs (**e**). Topaz was used to find more side views of GJIChs in the dataset of Cx43-WT GJICh in nanodiscs. See Methods for details.

Extended Data Fig. 2 | Validation of cryo-EM reconstruction maps.

a-c, Validation of cryo-EM maps of Cx43-WT GJICh at pH 8.0 in detergents (**a**) and in nanodiscs (**b**), and Cx43-M257 GJICh at pH 8.0 in detergents (**c**). Three representative 2D class averages (left). Cryo-EM maps colored according to local resolution estimated by ResMap (middle). The resolution range bars indicate local resolution gradients. Fourier shell correlation (FSC) curves between the two unfiltered half maps and between the model and the full map (right).

d,e, Representative map densities of NTH, the NTH-TM1 loop and TM1 in the Cx43-WT GJICh structure at pH 8.0 in the GCN state (**d**) and the Cx43-M257 GJICh structure at pH 8.0 in the PLN state (**e**), respectively. π-helix in the middle of TM1 is colored in black.

Extended Data Fig. 3 | Structural comparison of Cx43 GJICh with other GJIChs and Cx31.3 hemichannel.

a, Superposition of Cx43 in the GCN state with Cx26 (PDB accession code 2ZW3) (left) and Cx46 (PDB accession code 7JKC) (middle), and Cx31.3 hemichannel (PDB accession code 6L3T) (right). Cx43, Cx26, Cx46, and Cx31.3 are colored in green, gray, pink, and yellow, respectively. Two-way arrows indicate significant conformational differences of NTHs between two superposed connexins.

b, Detailed intermolecular interaction between NTH (magenta) and TM2 in a neighboring protomer (gray). This intermolecular interaction is relatively superficial compared with the tight intramolecular interaction shown in Fig. 2b. Residues involved in the interaction are drawn as sticks and labeled.

c, Superposition of Cx43 GJICh (green) and Cx31.3 hemichannel (yellow) structures both in the GCN conformation. The superposed structures are viewed from the membrane (left) and the cytoplasm (right) are shown. In the view from the membrane, only two protomers facing each other are shown for clarity. One-way arrows indicate conformational differences in the cytoplasmic regions of TM2 and TM3.

d, Close-up view of the space between two neighboring NTHs and TM2. Residues involved in the intramolecular NTH-TM2 interaction in the GCN state of Cx31.3 hemichannel are drawn as sticks and labeled. An arrow indicates substantial difference in the TM2 position between Cx43 and Cx31.3.

Extended Data Fig. 4 | Workflow of cryo-EM image processing of Cx43-M257 GJICh including localized reconstruction and focused classification on a single hemichannel.

Red circles indicate the selected particle classes or a reconstruction map for the next processes. Transparent blue, yellow and green masks in **a**, **c** and **d** indicate the regions selected for reconstruction and classification. See Methods for details.

Extended Data Fig. 5 | Conservation of π-helix in the middle of TM1 between Cx43 and Cx46 and possibly through the connexin family.

a, Structural similarity between Cx43 (left) and Cx46 (middle) in the PLN state. Only the region from NTH to TM1 is shown and compared for clarity. Two π-helices in the extracellular end and the middle of TM1 are indicated by lines and labeled in each of Cx43 and Cx46 structures. Cα root mean square deviation (RMSD) between the two superposed structures (right) is 1 Å.

b, Detailed view of 'W4 binding pocket': Close-up view of the region boxed in (A). 'W4 binding pocket' is formed by two TM1s and a TM2 at the interface between two neighboring protomers. On the ribbon drawings of NTH (magenta), TM1 and TM2 in one protomer (orange), and TM1 in the other protomer (gray), W4-interacting residues are drawn as sticks and labeled.

c-e, Structural comparison of the middle part of TM1 among Cx43 GCN (**c**), Cx43 PLN (**d**), and Cx46 (**e**) structures with map densities (meshes). π-helices are colored in black. The amide proton of I34 form a hydrogen-bonding (dotted line) with the carbonyl oxygen of F30 in the Cx43 GCN conformation, but with that of L29 in the Cx43 PLN conformation.

f, ConSurf analysis of Cx43. On a space filling model of Cx43 in the PLN state, amino acids are colored based on the degree of sequence conservation among 20 human connexin proteins, except the highly diversified member Cx23, from the most conserved (purple) to the least conserved (cyan). Three most conserved regions are indicated by dotted circles and labeled.

g, Sequence alignment of TM1s from 20 human connexin proteins. The π-helix-forming sequences confirmed by Cx43, Cx46, and Cx50 structures are indicated by red boxes. 100%

conserved positions are shaded in black, and >80% similarly conserved positions are in gray, respectively.

Extended Data Fig. 6 | Conformational changes in the NTH-TM1 loop and TM2–4 during the GCN-to-PLN transition.

a, Superposition of GCN (green) and PLN (orange) protomers of Cx43 GJICh to see the conformational change of the NTH-TM1 loop. Arrows and numbers indicate conformational changes of NTH (magenta) and TMs and the moving distances of the cytoplasmic ends of TMs.

b,c, Detailed structural comparison between GCN (**b**) and PLN (**c**) protomers at the boxed region in **a**. Residues participating in the interactions between loop and TMs are drawn as sticks and labeled.

d, Conformational changes of individual TMs (TM1–4) between GCN and PLN protomers. Individual TMs are separately shown. The bending angles between superposed helices are indicated by dashed lines and labeled. The first and the last residues of TMs are labeled.

e, Close-up view of the conformational change at the region boxed in **a**. Four residues (I31, V28, W25, and Y17) were selected to easily trace a series of conformational changes from π-helix to the NTH-TM1 loop and represented as sticks and labeled. One-way arrow indicates conformational shifts of the selected residues. Y17 is also shown as transparent space-filling models, and its interacting residues shown in **b** and **c** are represented as sticks.

f,g, Detailed interactions between neighboring protomers viewed from the inside of the pore of GCN (**f**) or PLN (**g**) hemichannel. NTHs are represented as magenta coils. GCN and PLN protomers are shown as ribbons. To distinguish between two protomers at their interface, one protomer on the left is colored in green in **f** or orange in **g**, and the other protomer on the right is colored in gray. Residues on the protomer-protomer interface are drawn as gray sticks and labeled.

h,i, Detailed interactions between neighboring protomers viewed from the outside of the pore of GCN (**h**) or PLN (**i**) hemichannel. Color codes are identical with those in **f** and **g**. Several representative residues showing dramatic conformational changes between GCN and PLN protomers are drawn as gray sticks and labeled. A dashed circle indicates the membrane opening between two protomers.

j,k, Close-up view of the intermolecular interfaces between GCN and PLN protomers in a mixed hemichannel. The residues lining the intermolecular interfaces are represented as space filling models to see any steric hindrance between two different protomers. The residues in π-helix are colored in gray.

Extended Data Fig. 7 | Dye transfer assays for mutant Cx43 GJIChs.

a, Rationale design of V24R and W25R mutations expected to disturb GCN and PLN conformations, respectively, but not the other way around.

b, Representative images to see the expression levels and the gap junction forming efficiencies of eCFP-fused Cx43-WT and the mutants. Arrows indicate gap junction plaques.

c, Representative images of scrape-loading dye-transfer assays with sulforhodamine B dye. The transiently expressed wild-type and mutant Cx43 proteins are labelled on the top of each image. Red fluorescence signals of sulforhodamine B spreading from the scrap line are shown. The spreading distances are indicated by arrows. Scale bar, 50 μm.

d, Hypothetical model of the transport of large molecules through Cx43 GJICh. Dyes and ATPs may be transported through a bigger pore (middle panel) formed by the dynamic GCN-to-PLN transition. I31A and L91A mutations may inhibit this conformational transition at the indicated transition steps.

Extended Data Fig. 8 | MD simulations of ion transfer through various Cx43 GJICh structures.

a,b, Local concentration maps and ionic fluxes of Na (**a**) and Cl (**b**) for fully GCN, mixed (3 consecutive PLNs and GCNs), and fully PLN GJIChs. No lipid is included inside the channels. MD simulations are conducted at a 200-mV transmembrane potential. Local concentrations of ions are represented as gray heat maps according to the gray scale indication bar on the right. Ionic fluxes are represented by arrows colored according to flux intensity indicated by the color bar on the right.

c, Local concentration maps and ionic fluxes of Na (left) and Cl (right) for fully GCN GJICh with lipids (CHSs and POPCs) embedded between NTHs and TM2s. MD simulations are conducted at a 200-mV transmembrane potential.

d,e, Comparison of the cytoplasmic entrances of two fully GCN GJICh models without (**d**) and with (**e**) lipids bound to NTHs, TM1s, and TM2s. The constriction sites are indicated and labeled. Diameters of the constriction sites and the surface of the pore pathway (cyan) was calculated and drawn using CAVER v.3.03. Lipid molecules (gray) in **e**, which are embedded in 6 holes between neighboring NTHs, are represented as space filling models.

Extended Data Fig. 1

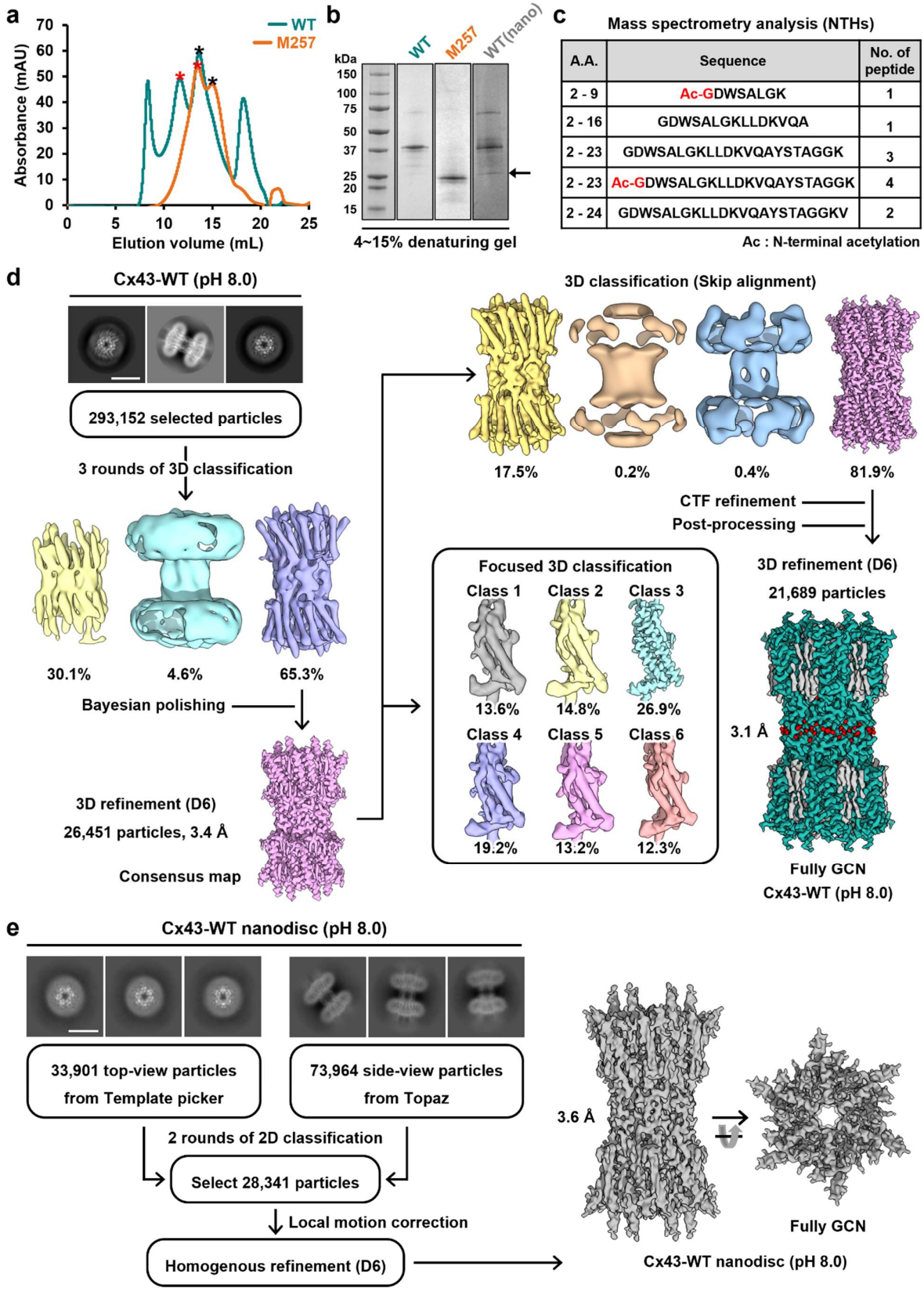

Extended Data Fig. 2

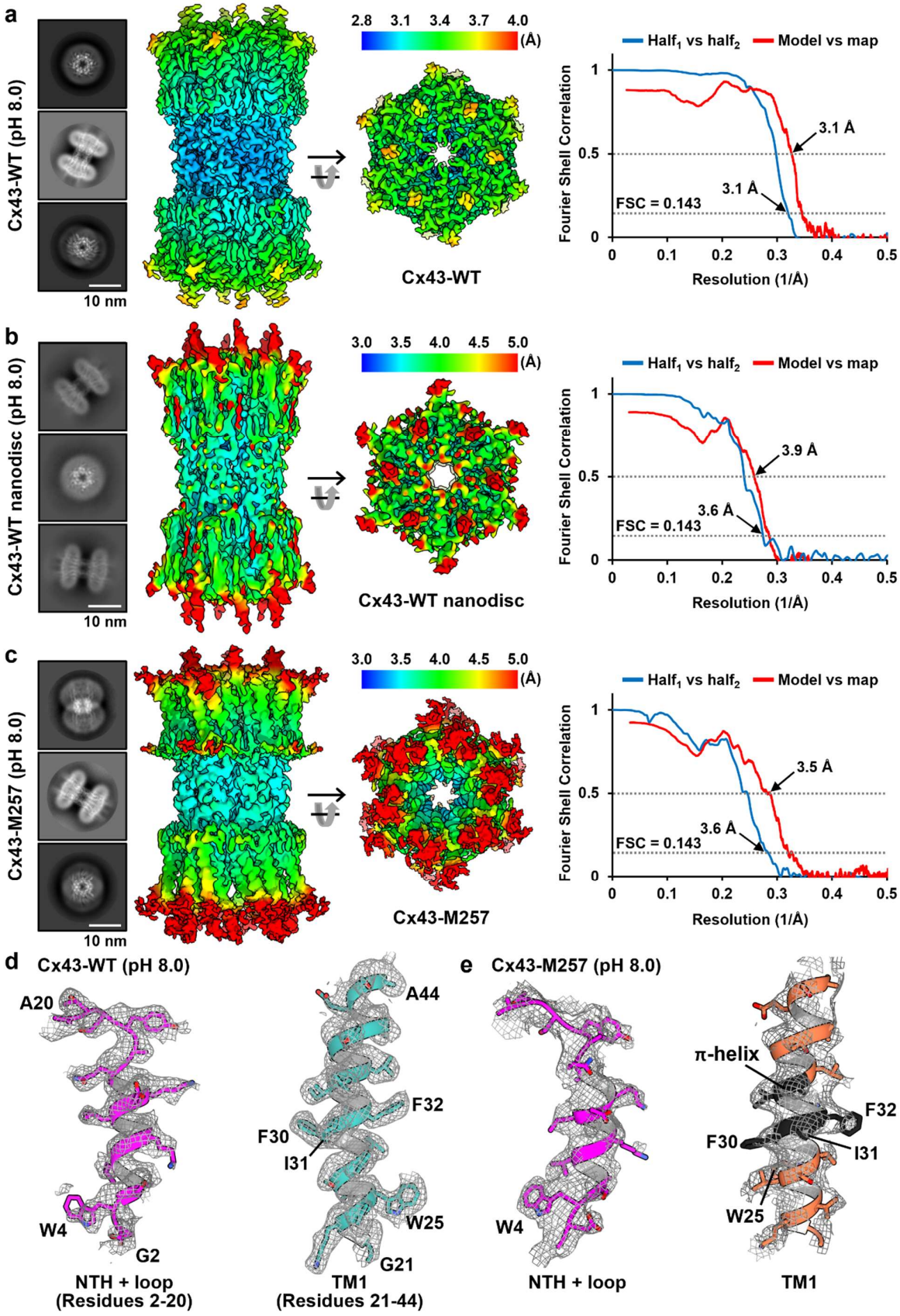

Extended Data Fig. 3

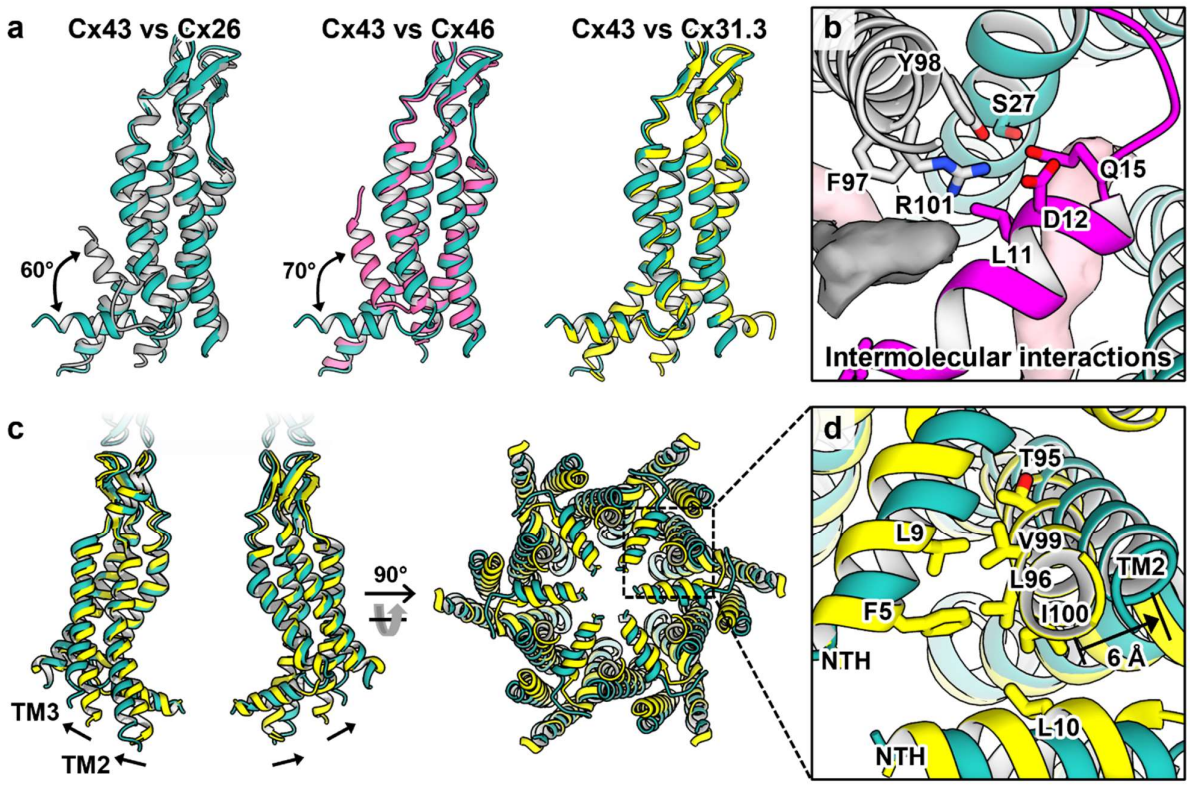

Extended Data Fig. 4

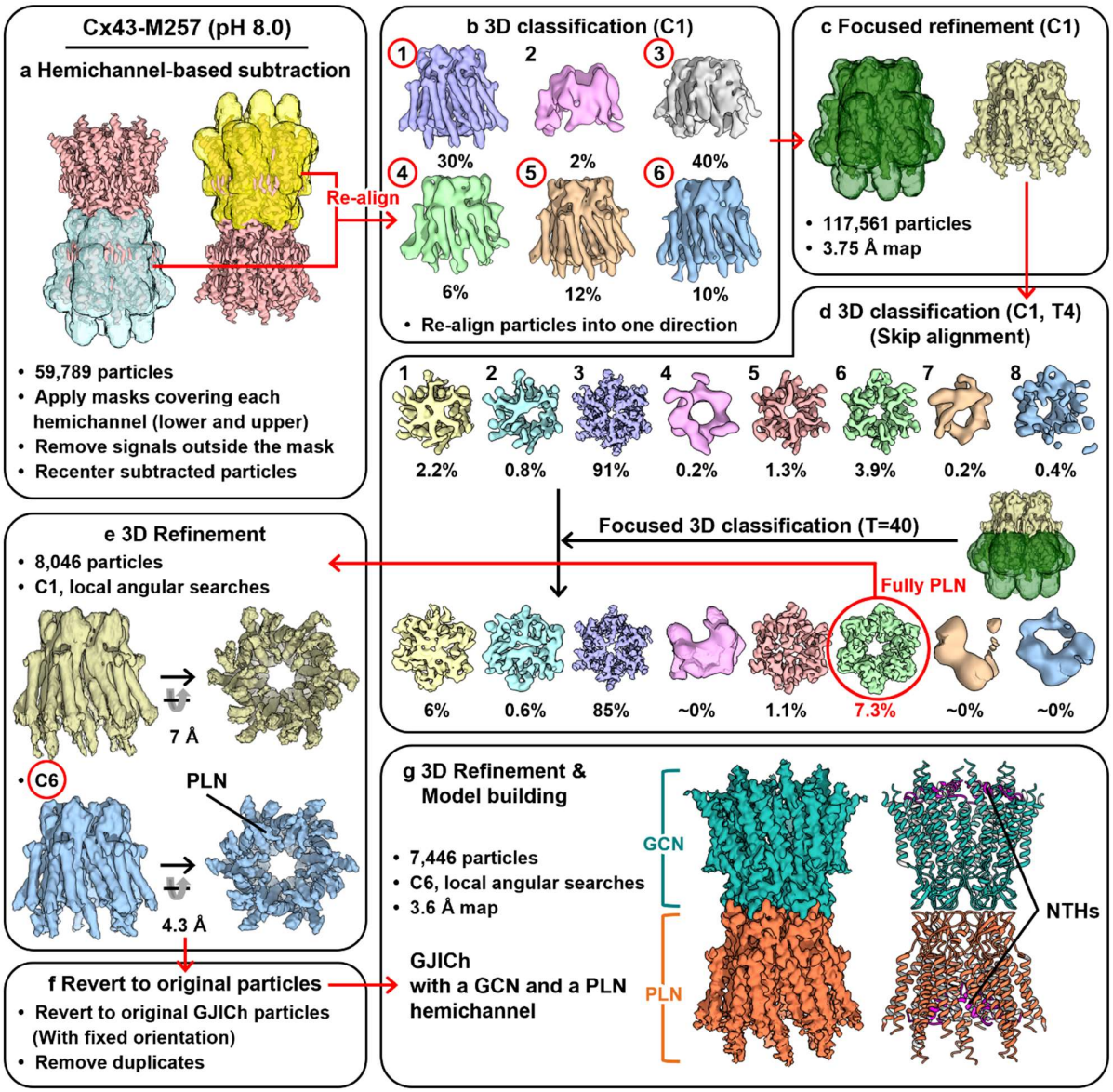

Extended Data Fig. 5

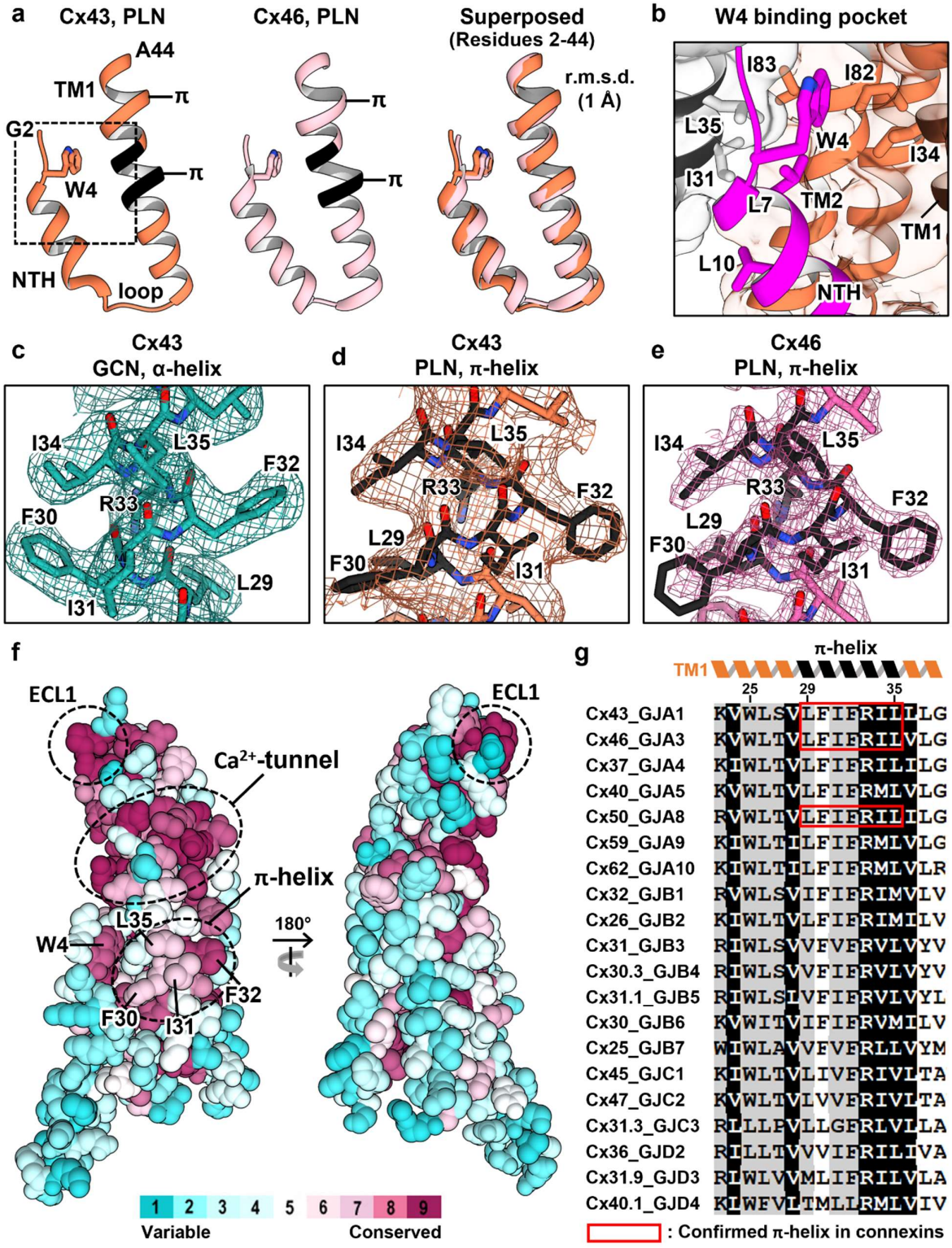

Extended Data Fig. 6

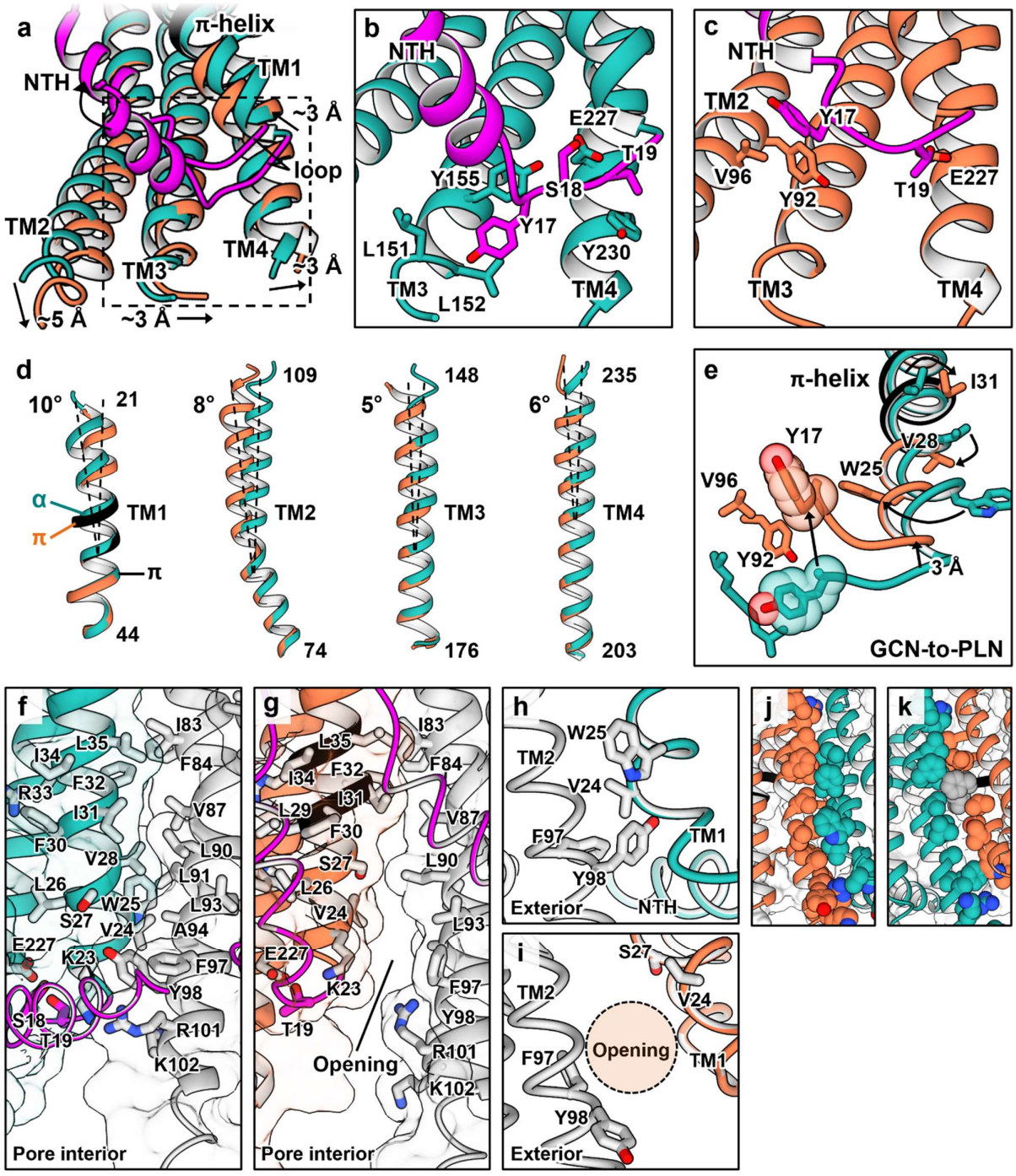

Extended Data Fig. 7

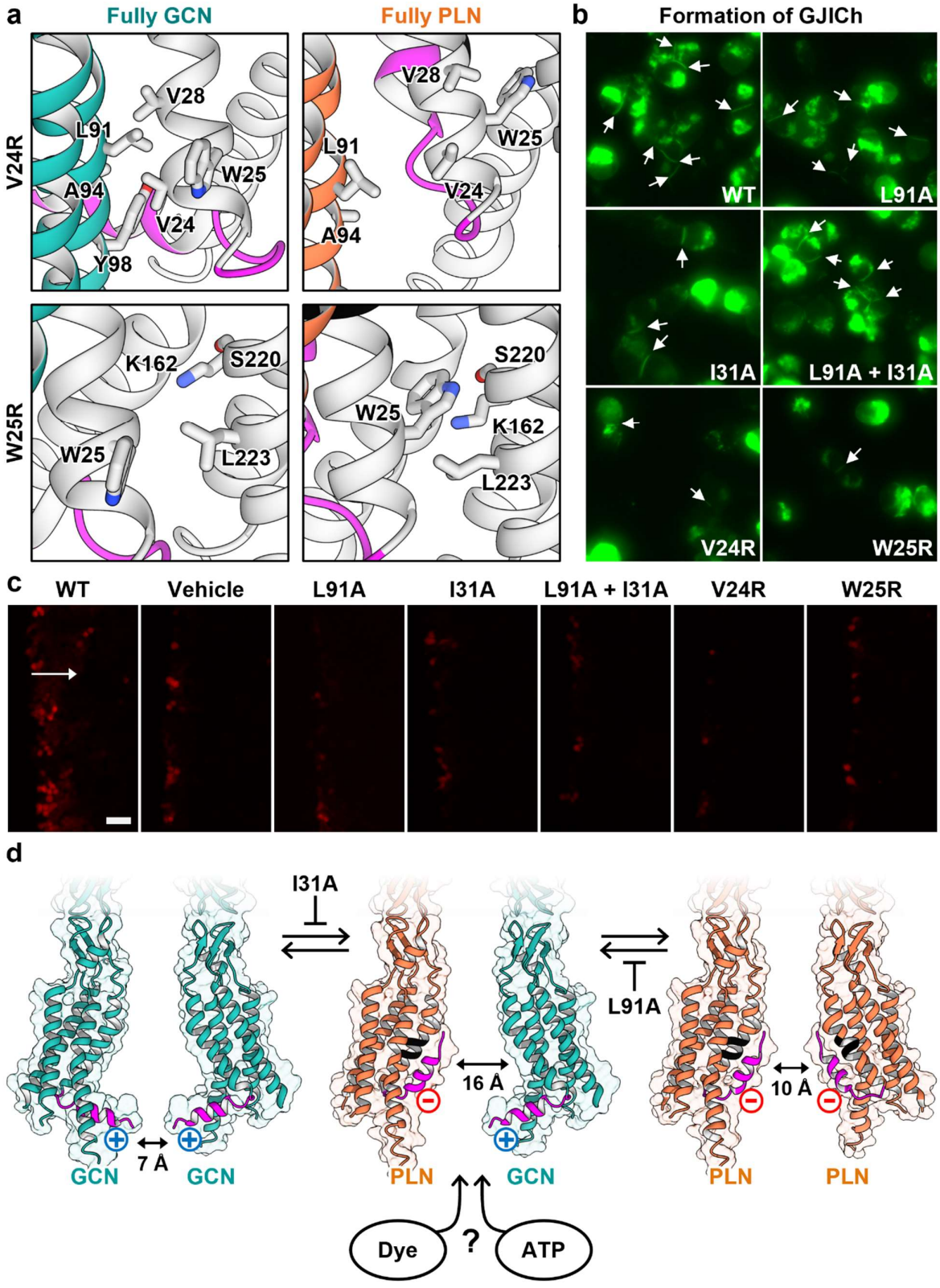

Extended Data Fig. 8